Inorg. Chem. **2003**, *42*, 5330–5339

Effect of Mono- versus Di-ammonium Cation of 2,2′-Bithiophene Derivatives on the Structure of Organic–Inorganic Hybrid Materials Based on Iodo Metallates

Xu-Hui Zhu,[†,||] Nicolas Mercier,*[,†] Pierre Frère,[‡] Philippe Blanchard,[‡] Jean Roncali,[‡] Magali Allain,[†] Claude Pasquier,[§] and Amédée Riou[†]

Ingénierie Moléculaire et Matériaux Organiques, UMR-CNRS 6501, Université d'Angers 2 Bd Lavoisier, 49045 Angers, France, Groupe Systèmes Conjugués Linéaires, IMMO, UMR 6501, Université d'Angers 2 Bd Lavoisier, 49045 Angers, France, and Laboratoire de Physique des Solides, UMR-CNRS 8502, Bât. 510,Université Paris Sud, 91405 Orsay, France

Received March 4, 2003

2,2′-bithiophene derivatives, 5-ammoniumethylsulfanyl-2,2′-bithiophene (AESBT) and 5,5′-bis(ammoniumethylsulfanyl)-2,2′-bithiophene (BAESBT), have been designed for their incorporation in organic–inorganic materials based on iodometalates. Three layered compounds, $(BAESBT)PbI_4$, $(AESBT)_4Pb_3I_{10}$, and $(AESBT)_3Bi_2I_9$, have been synthesized as crystals from slowly cooled aqueous solution containing metal halide and bithiophene derivative salts. When starting from the diammonium cation, $(BAESBT)PbI_4$ hybrid perovskite is obtained. $(BAESBT)PbI_4$ adopts a triclinic cell ($P\bar{1}$) with the lattice parameters $a = 8.4741(5)$ Å, $b = 8.9255(6)$ Å, $c = 16.876(1)$ Å, $\alpha = 88.328(5)°$, $\beta = 81.806(4)°$, $\gamma = 88.864(5)°$, $Z = 2$. In the structure, PbI_4^{2-} perovskite sheets and diammonium cation layers alternate along *c*. The incorporation of the corresponding monoammonium cation (AESBT) leads to a head to tail arrangement of the molecules in the $(AESBT)_4Pb_3I_{10}$ hybrid, precluding the formation of the perovskite layers. $(AESBT)_4Pb_3I_{10}$ is orthorhombic, $Pna2_1$, with $a = 38.333(4)$ Å, $b = 22.239(3)$ Å, $c = 8.448(2)$ Å, $Z = 4$. The structure consists of corrugated layers of $Pb_3I_{10}^{4-}$ separated by organic layers of monoammonium cations. A similar relative situation of molecules in organic layers is observed in $(AESBT)_3Bi_2I_9$, with the inorganic sheets being built up from $Bi_2I_9^{3-}$ entities. $(AESBT)_3Bi_2I_9$ crystallizes in an orthorhombic cell ($P2_12_12_1$) with $a = 8.4564(6)$ Å, $b = 21.368(2)$ Å, $c = 30.747(2)$ Å, $Z = 4$. In the three compounds, the molecular packings appear different, underlining the interplay between both organic and inorganic components. New packings are stabilized, as illustrated by an original mixed kappa–alpha type arrangement of the bithiophene units in $(AESBT)_3Bi_2I_9$. Furthermore, molecular interactions, especially of S...S type, appear stronger in the hybrids based on the monoammonium cations. The electrical conductivity of a $(BAESBT)PbI_4$ single crystal has also been investigated, revealing a semiconductive behavior with a characteristic energy of $E_g = 2.535$ eV.

Introduction

Considerable current interest focused on organized organic–inorganic perovskites is motivated by their unique combination of properties. On one hand the growth of single crystals allows a straightforward analysis of the relationships between the structure and the physical and electronic properties. On the other hand, their original electronic properties arising from their dual nature associated with their possible solution processing by room-temperature techniques such as spin-coating opens interesting perspectives for technological applications.

Hybrid perovskites generally consist of two-dimensional networks of corner-sharing divalent metal halide octahedra separated by an organic part involving either a bilayer of monoammonium cations or a monolayer of diammonium cations.[1] In most cases, the organic entities are alkyl- or simple aromatic ammonium cations[1,2−4] and behave as

* E-mail: nicolas.mercier@univ-angers.fr. Fax: 33.(2)0.41.73.54.05. Tel: 33.(2)0.41.73.50.83.
[†] Ingénierie Moléculaire et Matériaux Organiques.
[‡] Groupe Systèmes Conjugués Linéaires.
[§] Laboratoire de Physique des Solides.
[||] Current address: Institute of Advanced Materials, Fudan University, People's Republic of China.

(1) Mitzi, D. B. *Prog. Inorg. Chem.* **1999**, *48*, 1−121.

10.1021/ic034235y CCC: $25.00 © 2003 American Chemical Society
Published on Web 07/31/2003

weakly interacting individual molecules[1]; their large band gap also making them optically (in the visible spectrum) and electrically inert molecules. In addition to the control of the dimensionality, the organic layers also enhance the exciton binding energy associated with the inorganic component.[5,6] This property is responsible for the luminescence arising from the radiative decay of excitons. The combination of a strong luminescence and substantial carrier mobility has led to the fabrication of an efficient electroluminescent device.[7]

A recent trend in this field of hybrid materials consists of the incorporation of molecules with reduced HOMO−LUMO gap such as extended π-linear conjugated systems,[8] which can combine semiconducting properties,[9] and luminescent[10] or nonlinear optical[11] properties. For example, the bis-(ammonium-ethyl)quaterthiophene)PbX_4 perovskite exhibits a strong luminescence of the organic part when the HOMO−LUMO gap of the latter fits the VB−CB gap (X = Cl). In contrast, when the HOMO−LUMO and VB−CB levels shift from one another, (X = I), charge separation occurs and holes and electrons are collected by organic and inorganic components, respectively.[8] Thus, incorporation of π-conjugated systems in organic−inorganic hybrids provides a convenient method to control their intermolecular interactions to either avoid the quenching of luminescence associated with strongly interacting π-systems, or in contrast to strengthen these interactions to enhance hole mobility in the organic layer.

Among the few known layered perovskites including extended π-conjugated molecules, only the crystal structure of (AEQT)$PbBr_4$, based on a diammonium cation, has been reported.[8] The structure reveals a herringbone arrangement of the quaterthiophene units, and no intermolecular S...S distance smaller than 4.15 Å is observed. A possible strategy to modulate the molecular packing of such hybrid perovskites can consist of the replacement of diammonium cations by the corresponding monoammonium cation. Such an approach can be expected to provide more flexibility to the self-organization of the oligomer units.

Recently, we reported preliminary results on hybrid perovskite incorporating a single thiophene ring.[4] As a further step, we now report the synthesis and characterization of a monoammonium bithiophene derivative salt $(C_4S)_2S(CH_2)_2$-NH_3^+,Cl^- ((AESBT)Cl), and the related symmetrical diammonium salt $(NH_3(CH_2)_2S(C_4S)_2S(CH_2)_2NH_3)^{2+},2Cl^-$ ((BAESBT)Cl_2) (Chart 1). The effect of the charge and structure of the cationic bithiophene derivative has been investigated, and the results are discussed on the basis of the perspectives they open for the design and synthesis of new electronic materials.

Chart 1

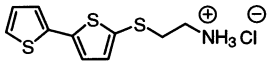

(AESBT)Cl

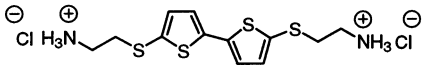

(BAESBT)Cl_2

Experimental Section

Synthesis. *(a) (AESBT)Cl Salt.* The intermediate 5-(2-phthalimidoethylsulfanyl)-2,2′-bithiophene (**1a**) was synthesized as follows. To a solution of 2,2′-bithiophene (1 g, 6 mmol) in anhydrous THF (40 mL) under N_2 at −78 °C, a solution of *n*-BuLi 2.5 M in hexane (2.50 mL, 1.05 equiv) was added dropwise over a period of 5 min. After 30 min of stirring at −78 °C the lithiated salt precipitated, and then elemental sulfur (0.20 g, 1.05 equiv) was added in one portion. After 30 min of additional stirring at −78 °C, the reaction mixture was allowed to warm to 0 °C and a solution of *N*-(2-bromoethyl)phthalimide (1.84 g, 1.2 equiv) in anhydrous THF (12 mL) was added dropwise. The mixture was stirred for 18 h at 20 °C and then concentrated in vacuo. After dilution with CH_2Cl_2 (200 mL), the solution was washed with water (75 mL), dried over $MgSO_4$, and evaporated in vacuo. The resulting blue oil was purified by two successive columns chromatography on silica gel (eluent, CH_2Cl_2) affording compound **1a** (1.30 g, 58% yield) as a white greenish solid. mp 114 °C. ^{1}H NMR (500 MHz, $CDCl_3$) δ: 3.13 (t, 2H, ^3J = 6.5 Hz), 3.96 (t, 2H, ^3J = 6.5 Hz), 6.96 (d, 1H, ^3J = 3.7 Hz), 7.00 (dd, 1H, ^3J = 5.0 Hz, ^3J = 3.5 Hz), 7.11 (d, 1H, ^3J = 3.5 Hz), 7.15 (d, 1H, ^3J = 3.7 Hz), 7.21 (d, 1H, ^3J = 5.0 Hz), 7.68−7.72 (m, 2H), 7.81−7.85 (m, 2H). ^{13}C NMR (125 MHz, $CDCl_3$) δ: 36.5, 37.5, 123.3, 123.8, 124.1, 124.8, 127.8, 131.8, 131.9, 134.0, 135.5, 136.8, 141.4, 168.2. MS (70 eV, EI) *m*/*z* (I%): 169 ($M^{+\bullet}$, 53), 129 (54), 116 (29), 85 (50), 71 (100). IR (KBr) ν cm^{-1} : 1767 and 1716 (C═O).

The preparation of 5-ammoniumethylsulfanyl-2,2′-bithiophene chloride salt (AESBT)Cl was achieved by refluxing for 3 h a mixture of compound **1a** (1.22 g, 3.3 mmol) and hydrazine 80% in water (1 mL) in a 1:1 mixture of solvents THF/EtOH (40 mL). At room temperature, the white precipitate was separated by filtration, and the filtered solution was concentrated in vacuo. After addition of CH_2Cl_2 (150 mL) to the residue, the solution was washed with an aqueous saturated solution of Na_2CO_3, dried over $MgSO_4$, and then evaporated in vacuo affording the free amine as a colorless oil (0.79 g). This oil was directly used in the next step without further purification. Thus, it was dissolved in $CHCl_3$ (30 mL), and an aqueous solution of HCl 6 N (3 mL) was added dropwise leading to a white precipitate which was recovered by filtration and washed with $CHCl_3$. Compound (AESBT)Cl was obtained as a white solid (0.87 g, 95% yield). mp 208 °C. ^{1}H NMR (500 MHz, CD_3SOCD_3) δ: 2.94 (t, 2H, ^3J = 7.3 Hz), 3.08 (t, 2H, ^3J = 7.3 Hz), 7.08 (dd, 1H, ^3J = 5.1 Hz, ^3J = 3.6 Hz), 7.23 (d, 1H, ^3J = 3.7 Hz), 7.28 (d, 1H, ^3J = 3.7 Hz), 7.31 (dd, 1H, ^3J = 3.6 Hz and ^3J = 1.0 Hz), 7.53 (dd, 1H, ^3J = 5.1 Hz and ^3J = 1.0 Hz), 8.37 (br. s, 3H). IR (KBr) ν cm^{-1}: 2900 (NH_3^+).

(2) Papavassiliou, G. C.; Koutselas, I. B.; Terzis, A.; Whangbo, M. H. *Solid State Commun.* **1994**, *91*, 965.
(3) Papavassiliou, G. C.; Mousdis, G. A.; Raptopoulo, C. P.; Terzis, A. *Z. Naturforschung* **1999**, *54b*, 1405.
(4) Zhu, X. H.; Mercier, N.; Riou, A.; Blanchard, P.; Frère, P. *Chem. Commun.* **2002**, *8*, 2160−2161.
(5) Hong, X.; Ishihara, T.; Nurmikko, A. V. *Phys. Rev. B* **1992**, *45*, 6961.
(6) Ishihara, T. *J. Lumin.* **1994**, 60/61, 269.
(7) Era, M.; Morimoto, S.; Tsutsui, T.; Saito, A. *Appl. Phys. Lett.* **1994**, *65*, 676.
(8) Mitzi, D. B.; Chondroudis, K.; Kagan, C. R. *Inorg. Chem.* **1999**, *38*, 6246.
(9) (a) Dimitrakopolous, C. D.; Malenfant, P. *Adv. Mater.* **2002**, *14*, 99. (b) Katz, H. E.; Bao, Z.; Gilat, S. *Acc. Chem. Res.* **2001**, *34*, 359. (c) Garnier, F. *Acc. Chem. Res.* **1999**, *32*, 209. (d) Horowitz, G. *Adv. Mater.* **1998**, *10*, 365.
(10) (a) Kraft, A.; Grimsdale, A. C.; Holmes, A. B. *Angew. Chem. Int. Ed.* **1998**, *37*, 402. (b) Mitschke, U.; Bäuerle, P. *J. Mater. Chem.* **2000**, *10*, 1471−1507.
(11) (a) Prasad, P. N.; Williams, D. J. *Introduction to Nonlinear Optical Effects in Molecules and Polymers*; Wiley: New York, 1991. (b) Zyss, J. *Molecular Nonlinear Optics: Materials, Physics and Devices*; Academic Press: Boston, MA, 1993.

Table 1. Crystallographic Data for (BAESBT)PbI_4, $(AESBT)_4Pb_3I_{10}$, and $(AESBT)_3Bi_2I_9$

	(BAESBT)PbI_4	$(AESBT)_4Pb_3I_{10}$	$(AESBT)_3Bi_2I_9$
empirical formula	$C_{12}H_{18}I_4N_2PbS_4$	$C_{40}H_{48}I_{10}N_4Pb_3S_{12}$	$C_{30}H_{36}Bi_2I_9N_3S_9$
Fw (g/mol)	1033.31	2860.11	2287.22
crystal size (mm^3)	$0.44 \times 0.22 \times 0.03$	$0.65 \times 0.10 \times 0.10$	$0.60 \times 0.19 \times 0.08$
space group	$P\bar{1}$ (No. 2)	$Pna2_1$ (No. 33)	$P2_12_12_1$ (No.19)
a, Å	8.4741(5)	38.333(4)	8.4564(6)
b, Å	8.9255(6)	22.239(3)	21.368(2)
c, Å	16.8760(10)	8.448(2)	30.747(2)
α, °	88.328(5)	90	90
β, °	81.806(4)	90	90
γ, °	88.864(5)	90	90
V, $Å^3$	1262.7(1)	7202(2)	5555.9(7)
Z	2	4	4
ρ_{calc}, g/cm^3	2.718	2.638	2.734
abs. coeff, mm^{-1}	11.90	11.66	11.69
obs. reflns ($I > 2\sigma(I)$) / parameters	3158/229	4108/420	9070/476
R1/wR2 ($I > 2\sigma(I)$)	0.037/0.099	0.058/0.143	0.045/0.114

(b) (BAESBT)Cl_2 Salt. A solution of 2,2′-bithiophene (2 g, 12 mmol) in THF (40 mL) was treated with *n*-BuLi 1.6 M in hexane (15.8 mL, 2.1 equiv) at −78 °C and the resulting lithium salts precipitated from the solution. The reaction mixture was left to warm to room temperature and stirred for 1 h. Sulfur (0.80 g, 2.1 equiv) was added in one portion to give a yellow precipitate and the reaction mixture was stirred for another 1 h, followed by addition of *N*-(2-bromoethyl)phthalimide (6.7 g, 2.2 equiv) at 0 °C. After the mixture was stirred overnight, water was added and CH_2Cl_2 was used to extract the solid. The organic phase was dried in anhydrous $MgSO_4$ and evaporated to dryness. The residue was triturated in boiling acetone (50 mL) and filtered to afford 5,5′-bis(2-phthalimidoethylsulfanyl)-2,2′-bithiophene **1b** as a pure yellow solid (3.5 g, 50% yield). mp 204 °C. MS MALDI-TOF calculated for $C_{28}H_{20}N_2O_4S_4$, 576.03; found, 576.02. ^{1}H NMR (500 MHz, $CDCl_3$) δ: 3.13 (t, 4H), 3.95 (t, 4H), 6.87 (d, 2H, $^3J = 3.65$ Hz), 7.11 (d, 2H, $^3J = 3.67$ Hz), 7.70 (q, 4H), 7.83(q, 4H). ^{13}C NMR (125 MHz, $CDCl_3$) δ: 36.5, 37.6, 123.3, 124.1, 132.0, 132.6, 134.0, 135.2, 140.6, 168.1. IR (KBr) ν cm^{-1} : 1770 and 1712 (C═O).

Compound **1b** (1.8 g, 3.1 mmol) was dissolved in a hot mixture of chloroform and ethanol to get a clear solution, and then excessive hydrazine 80% in water was added. Within 1 h, a white precipitate formed and the reaction mixture continued to reflux overnight. The solid was filtered off and the filtrate was evaporated to dryness to give an oily residue which was redissolved in THF. This solution was washed with water, and dried over anhydrous $MgSO_4$. The organic phase was filtered and bis-ammonium salt (BAESBT)Cl_2 was precipitated upon addition of an aqueous solution of HCl 6 N affording, after being washed with DMF and acetone, a yellow solid (0.8 g, 60% yield). mp > 260 °C. ^{1}H NMR (500 MHz, D_2O) δ: 2.98 (t, 4H), 3.08 (t, 4H), 7.70 (q, 4H), 7.06 (d, 2H, $^3J = 3.80$ Hz), 7.09 (d, 2H, $J = 3.79$ Hz). IR (KBr) ν cm^{-1}: 2920 (NH_3^+).

(c) (BAESBT)PbI4 Crystals. A mixture of (BAESBT)Cl_2 (12.8 mg, 0.03 mmol), PbI_2 (15 mg, 0.033 mmol), excess KI (7 g), one drop of concentrated HI, and H_2O (10 mL) was sealed in a Pyrex tube and kept at the temperature of 90 °C for 1 h and then at 110 °C for 4 h. Subsequent cooling to room temperature at 2 °C/h resulted in well formed orange plate single crystals, with a size of $(2 \times 2 \times 0.2)$ mm^3 for the biggest ones. Powder XRD pattern (given as Supporting Information) shows the bulk sample belongs to the same phase.

(d) (AESBT)4Pb3I10 Crystals. A mixture of (AESBT)Cl (9.7 mg, 0.037 mmol), PbI_2 (12.8 mg, 0.028 mmol), three drops of concentrated HI, and H_2O (4 mL) was sealed in a Pyrex tube and kept at the temperature of 100 °C for 4 h and then cooled to room temperature at 2 °C/h affording well formed yellow needle single crystals. The powder XRD pattern (given as Supporting Information) showed that the bulk sample belongs to the same phase.

(e) (AESBT)3Bi2I9 Crystals. A mixture of (AESBT)Cl (16.7 mg, 0.06 mmol), $BiCl_3$ (18.5 mg, 0.028 mmol), excess KI (1 g), two drops of concentrated HI and H_2O (5 mL) was sealed in a Pyrex tube and kept at the temperature of 100 °C for 10 h and then cooled to room temperature at 2 °C/h leading to well formed red plate single crystals. Powder XRD (given as Supporting Information) shows the bulk sample belongs to the same phase.

X-ray Crystallography. X-ray diffraction data of selected single crystals were collected on an Enraf-Nonius MACH3 four-circle diffractometer, for (BAESBT)PbI_4 and $(AESBT)_4Pb_3I_{10}$, and on a STOE-IPDS diffractometer for $(AESBT)_3Bi_2I_9$, both using graphite-monochromated Mo Kα radiation ($\lambda = 0.71073$ Å). A summary of crystallographic data and results of refinements is given in Table 1. All the three structures were solved and refined using the Shelxl97 package. Generally, heavy atoms (Pb, Bi, I) were first located using direct methods, C, S and N atoms were then located from the analysis of the Fourier difference maps. All hydrogen atoms were treated with a riding model. Positions and anisotropic thermal motion parameters of the non-H atoms were refined by full-matrix least-squares routines against F^2. Absorption effects were corrected using the Gauss method for two of the structures, and the psi-scan method was used for $(AESBT)_4Pb_3I_{10}$. For the non centrosymmetrical structures, the Flack parameter[12] converges to 0.12(2) and 0.088(5) for $(AESBT)_4Pb_3I_{10}$ and $(AESBT)_3Bi_2I_9$, respectively. In (BAESBT)PbI_4, a positional disorder is evidenced for one of the two centrosymmetrical molecules. The disorder affects four of the eight non-H atoms of the independent half molecule: the sulfur atom of the thiophene ring, the carbon atoms in 3 and 4 positions, and the other sulfur atom were each one located on two positions, an identical occupation rate being refined for atoms belonging to the same component. The major component, involving S4, C10, C11, and S3, comprises 67%.

Selected bond distances and angles for (BAESBT)PbI_4, $(AESBT)_4Pb_3I_{10}$, and $(AESBT)_3Bi_2I_9$ are provided in Tables 2−4. A complete list of crystallographic data, along with the atomic coordinates and the anisotropic motion parameters for each compound, is given as Supporting Information.

Physical Properties. Absorption spectra were obtained at room temperature on films of (BAESBT)PbI_4, $(AESBT)_4Pb_3I_{10}$, and $(AESBT)_3Bi_2I_9$, using a lambda 19 Perkin-Elmer spectrometer. These crystallized films could be prepared by the spin-coating technique after dissolution of the corresponding crystals in aceto-

(12) Flack, H. D. *Acta Crystallogr.* **1983**, A39, 876.

Table 2. Selected Bond Distances (Å) and Angles (°) for $(BAESBT)PbI_4$[a]

Pb(1)−I(3)	3.1499(6)	Pb(2)−I(3)#4	3.1665(6)
Pb(1)−I(1)	3.1733(10)	Pb(2)−I(4)	3.1958(6)
Pb(1)−I(4)	3.2106(6)	Pb(2)−I(2)	3.2010(9)
I(3)#3−Pb(1)−I(3)	180.0	I(3)#4−Pb(2)−I(3)#5	180.0
I(3)#3−Pb(1)−I(1)	90.86(2)	I(3)#4−Pb(2)−I(4)	84.81(2)
I(3)−Pb(1)−I(1)	89.14(2)	I(3)#5−Pb(2)−I(4)	95.19(2)
I(1)#3−Pb(1)−I(1)	180.0	I(3)#4−Pb(2)−I(2)#6	90.83(2)
I(3)#3−Pb(1)−I(4)	87.57(2)	I(3)#5−Pb(2)−I(2)#6	89.17(2)
I(3)−Pb(1)−I(4)	92.43(2)	I(4)−Pb(2)−I(2)#6	91.46(2)
I(1)#3−Pb(1)−I(4)	91.11(2)	I(4)#6−Pb(2)−I(2)#6	88.54(2)
I(1)−Pb(1)−I(4)	88.89(2)	I(2)#6−Pb(2)−I(2)	180.0
I(4)−Pb(1)−I(4)#3	180.0	I(4)−Pb(2)−I(4)#6	180.0
Pb(2)−I(4)−Pb(1)	151.87(3)	Pb(1)−I(3)−Pb(2)#7	149.40(3)

[a] #3 $-x, -y, -z$. #4 $-x-1, -y, -z$. #5 $x, y-1, z$. #6 $-x-1, -y-1, -z$. #7 $x, y+1, z$.

Table 3. Selected Bond Distances (Å) and Angles (°) for $(AESBT)_4Pb_3I_{10}$[a]

Pb(1)−I(4)	3.287(3)	Pb(2)−I(8)	3.166(2)
Pb(1)−I(5)	3.305(3)	Pb(2)−I(3)	3.167(2)
Pb(1)−I(3)	3.250(2)	Pb(2)−I(6)	3.176(3)
Pb(1)−I(2)	3.149(3)	Pb(2)−I(5)	3.278(3)
Pb(1)−I(1)	3.122(3)	Pb(2)−I(7)	3.278(3)
Pb(1)−I(10)#3	3.101(3)	Pb(2)−I(4)	3.176(3)
Pb(3)−I(2)#4	3.104(2)	I(8)−Pb(2)−I(3)	169.95(9)
Pb(3)−I(9)	3.132(3)	I(8)−Pb(2)−I(4)	83.96(7)
Pb(3)−I(8)	3.247(2)	I(3)−Pb(2)−I(4)	89.50(7)
Pb(3)−I(6)	3.274(3)	I(8)−Pb(2)−I(6)	89.38(7)
Pb(3)−I(10)	3.159(3)	I(3)−Pb(2)−I(6)	83.44(7)
Pb(3)−I(7)	3.307(3)	I(4)−Pb(2)−I(6)	93.82(8)
		I(8)−Pb(2)−I(7)	83.30(7)
I(10)#3−Pb(1)−I(1)	92.19(7)	I(3)−Pb(2)−I(7)	103.39(7)
I(10)#3−Pb(1)−I(2)	90.53(7)	I(4)−Pb(2)−I(7)	167.12(7)
I(1)−Pb(1)−I(2)	92.58(7)	I(6)−Pb(2)−I(7)	87.95(7)
I(10)#3−Pb(1)−I(3)	89.39(7)	I(8)−Pb(2)−I(5)	103.57(7)
I(1)−Pb(1)−I(3)	177.34(10)	I(3)−Pb(2)−I(5)	83.78(7)
I(2)−Pb(1)−I(3)	85.27(6)	I(4)−Pb(2)−I(5)	88.20(7)
I(10)#3−Pb(1)−I(4)	171.95(9)	I(6)−Pb(2)−I(5)	167.04(7)
I(1)−Pb(1)−I(4)	92.01(7)	I(7)−Pb(2)−I(5)	92.93(8)
I(2)−Pb(1)−I(4)	82.42(6)		
I(3)−Pb(1)−I(4)	86.17(6)	I(2)#4−Pb(3)−I(9)	93.20(6)
I(10)#3−Pb(1)−I(5)	100.14(9)	I(2)#4−Pb(3)−I(10)	90.25(7)
I(1)−Pb(1)−I(5)	99.72(8)	I(9)−Pb(3)−I(10)	92.95(8)
I(2)−Pb(1)−I(5)	163.32(6)	I(2)#4−Pb(3)−I(8)	88.86(5)
I(3)−Pb(1)−I(5)	82.09(7)	I(9)−Pb(3)−I(8)	177.05(10)
I(4)−Pb(1)−I(5)	85.91(7)	I(10)−Pb(3)−I(8)	84.91(7)
		I(2)#4−Pb(3)−I(6)	171.76(8)
Pb(2)−I(4)−Pb(1)	76.41(6)	I(9)−Pb(3)−I(6)	91.39(7)
Pb(2)−I(7)−Pb(3)	74.95(6)	I(10)−Pb(3)−I(6)	82.68(8)
Pb(2)−I(5)−Pb(1)	74.79(6)	I(8)−Pb(3)−I(6)	86.32(6)
Pb(3)#1−I(2)−Pb(1)	136.59(7)	I(2)#4−Pb(3)−I(7)	100.06(8)
Pb(1)#2−I(10)−Pb(3)	136.85(10)	I(9)−Pb(3)−I(7)	100.09(8)
Pb(2)−I(8)−Pb(3)	77.32(5)	I(10)−Pb(3)−I(7)	162.82(8)
Pb(2)−I(3)−Pb(1)	77.06(5)	I(8)−Pb(3)−I(7)	81.61(7)
Pb(2)−I(6)−Pb(3)	76.79(6)	I(6)−Pb(3)−I(7)	85.85(7)

[a] #1 $-x+3/2, y-1/2, z+1/2$. #2 $-x+3/2, y+1/2, z+1/2$. #3 $-x+3/2, y-1/2, z-1/2$. #4 $-x+3/2, y+1/2, z-1/2$.

nitrile, and the XRD patterns well-demonstrated the obtention of the expected phases only.

Conductivity measurements were obtained on single crystals of $(BAESBT)PbI_4$ with cooling below room temperature. A two-probes technique was used with gold contacts evaporated on the surface of the single crystal. The conductance was measured with a Keithley K487 picoammeter.

Results and Discussion

Synthetic Issues. Compounds (AESBT)Cl and $(BAESBT)Cl_2$ were prepared starting from 2,2′-bithiophene which was synthesized according to the Kumada procedure.[13]

Table 4. Selected Bond Distances (Å) and Angles (°) for $(AESBT)_3Bi_2I_9$

Bi(1)−I(4)	2.9355(10)	Bi(2)−I(7)	2.8895(10)
Bi(1)−I(5)	2.9357(10)	Bi(2)−I(9)	2.9403(9)
Bi(1)−I(6)	2.9428(10)	Bi(2)−I(8)	2.9845(11)
Bi(1)−I(2)	3.2242(9)	Bi(2)−I(2)	3.2000(9)
Bi(1)−I(1)	3.2551(4)	Bi(2)−I(3)	3.2008(10)
Bi(1)−I(3)	3.2914(9)	Bi(2)−I(1)	3.3659(5)
I(4)−Bi(1)−I(5)	92.82(3)	I(7)−Bi(2)−I(9)	92.71(3)
I(4)−Bi(1)−I(6)	95.95(3)	I(7)−Bi(2)−I(8)	95.59(3)
I(5)−Bi(1)−I(6)	96.83(3)	I(9)−Bi(2)−I(8)	93.40(3)
I(4)−Bi(1)−I(2)	87.89(3)	I(7)−Bi(2)−I(2)	94.56(3)
I(5)−Bi(1)−I(2)	170.81(3)	I(9)−Bi(2)−I(2)	172.13(3)
I(6)−Bi(1)−I(2)	92.21(3)	I(8)−Bi(2)−I(2)	88.89(3)
I(4)−Bi(1)−I(1)	90.97(2)	I(7)−Bi(2)−I(3)	89.31(3)
I(5)−Bi(1)−I(1)	86.58(2)	I(9)−Bi(2)−I(3)	93.18(3)
I(6)−Bi(1)−I(1)	172.11(2)	I(8)−Bi(2)−I(3)	171.60(3)
I(2)−Bi(1)−I(1)	84.25(2)	I(2)−Bi(2)−I(3)	83.91(2)
I(4)−Bi(1)−I(3)	169.71(3)	I(7)−Bi(2)−I(1)	174.24(3)
I(5)−Bi(1)−I(3)	96.68(3)	I(9)−Bi(2)−I(1)	89.63(2)
I(6)−Bi(1)−I(3)	86.87(3)	I(8)−Bi(2)−I(1)	89.52(3)
I(2)−Bi(1)−I(3)	82.10(2)	I(2)−Bi(2)−I(1)	82.85(2)
I(1)−Bi(1)−I(3)	85.67(2)	I(3)−Bi(2)−I(1)	85.30(2)
Bi(2)−I(3)−Bi(1)	79.07(2)	Bi(2)−I(2)−Bi(1)	80.09(2)
Bi(1)−I(1)−Bi(2)	77.24(1)		

Successive treatments of 2,2-bithiophene with one or two equivalents of *n*-BuLi at low temperature followed by addition of sulfur and further reaction with *N*-(2-bromoethyl)-phthalimide led, respectively, to compounds **1a** (58% yield) and **1b** (50% yield). The straightforward deprotection of the amino group(s) was carried out in the presence of hydrazine hydrate, and the resulting free amine compounds were directly converted to the corresponding ammonium salts by reaction with hydrochloric acid to give ammonium salts (AESBT)Cl and $(BAESBT)Cl_2$ in 95% and 60% overall yields, respectively.

The synthesis of the hybrid materials was accomplished with an improved method, starting directly from the chloride salts (AESBT)Cl or $(BAESBT)Cl_2$, and by using an excess of KI instead of a concentrated HI solution, thus avoiding experiments under inert atmosphere or evacuation/cooling in sealing the tube.

Crystal Structures. The crystal structures of $(BAESBT)PbI_4$, $(AESBT)_4Pb_3I_{10}$, and $(AESBT)_3Bi_2I_9$ can be first described as layered structures where the organic layers and inorganic sheets alternate along a main axis of the cell. Ionic bonds ensure the cohesion of the solid, together with hydrogen interactions, these latter being actually essential in the relative interplay of the two components at the organic−inorganic interface.

$(BAESBT)PbI_4$. The crystal structure of $(BAESBT)PbI_4$ consists of perovskite-type inorganic sheets separated by organic layers of diammonium cations, as encountered in hybrid compounds based on iodoplumbate and suitable primary ammonium cations (Figure 1). Each lead atom is surrounded by a slightly distorted octahedral coordination of iodide (Table 2), with bond lengths ranging from 3.150(1) Å to 3.210(1) Å and 3.167(1) Å to 3.201(1) Å for Pb(1) and Pb(2) respectively, while I−Pb−I bond angles range from 87.6(1)° to 92.4(1)° for Pb(1), and 84.8(1)° to 95.2(1)° for Pb(2), taking into account the two relative adjacent

(13) Tamao, K.; Kodoma, S.; Nakajima, I.; Kumada, M.; Minato, A.; Suzuki, K. *Tetrahedron* **1982**, *38*, 3347.

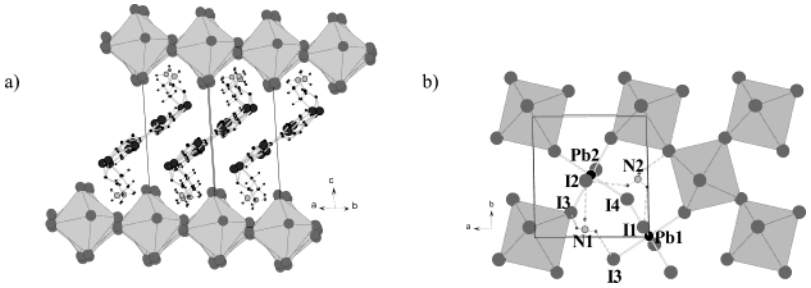

Figure 1. (a) Layered crystal structure of (BAESBT)PbI_4; (b) PbI_4^{2-} sheet and hydrogen bond interactions at the organic−inorganic interface (*d*(H...I) in the range 2.86−3.08 Å).

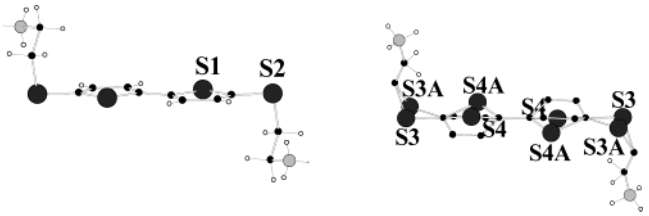

Figure 2. View of the two independent molecules of the (BAESBT)PbI_4 structure showing the anti conformation and the disorder for one of the two molecules.

iodine atoms of a polyhedron. All these values are close to those encountered in $(C_4H_3SCH_2NH_3)_2PbI_4$[4] and $(C_4H_9NH_3)_2PbI_4$[14] for instance. Also, the Pb−I−Pb bond angles in the equatorial plane, substantially different from 180° (149.4(1)° and 151.9(1)°), indicate a rotation of adjacent polyhedra in the sheet, which is well-known in hybrid perovskites.

The asymmetric unit contains two independent half-molecules. A treatment of a disorder which affects four of the eight non-H atoms of one of the independent half molecules, leads to define two components, the major one comprising 67% (see Experimental Section and Figure 2). The pair of thiophene rings in the two molecules are nearly planar, with dihedral angles of 1° and 5° between least-squares best planes containing adjacent thiophene rings, and adopt an anti conformation (Figure 2). The sulfur atoms linked to the thiophene units are nominally in the plane of bithiophene molecules, the ethylammonium tail being directed out of this plane, as evidenced in Figure 2. The $S(C_2H_5)NH_3^+$ tethering groups certainly involve some geometric constraints, leading finally to the uncommon observed low symmetry: (i) the inorganic sheets are corrugated with equatorial iodine atoms out of the (a, b) plane (Figure 1a); (ii) a dihedral angle of 41.4° is found between the bithiophene plane and the perovskite plane (Figure 1a); (iii) the hydrogen bonding provides two kinds of configuration, a so-called "terminal halogen configuration"[1] for N(2) (two H...$I_{terminal}$ interactions of three), and a so-called "bridging halogen configuration"[1] for N(1) (two H...$I_{bridging}$ interactions of three) (Figure 1b).

$(AESBT)_4Pb_3I_{10}$. The layered crystal structure of $(AESBT)_4Pb_3I_{10}$ is built up from 2D inorganic sheets surrounded by organic layers (Figure 3). As clearly shown in Figure 3, the hybrid perovskite, with $(AESBT)_2PbI_4$ hypothetical formula, is here not formed, although the chosen organic monofunctional cation was suitable for the incorporation in perovskite,

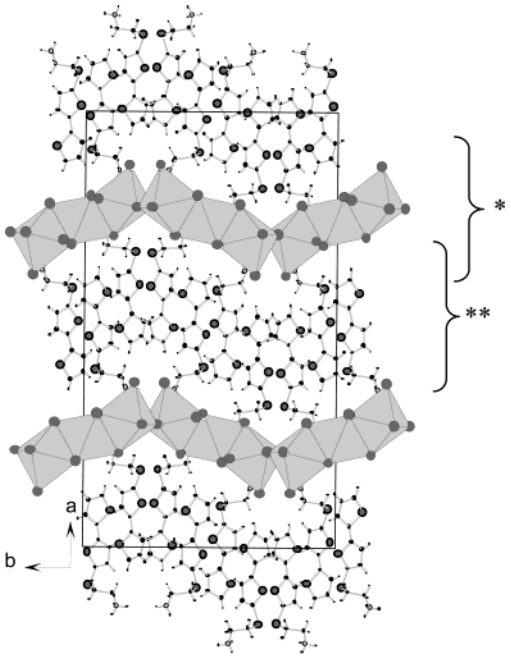

Figure 3. Layered crystal structure of $(AESBT)_4Pb_3I_{10}$. The brackets indicate the parts of the structure projected along [−1 0 0] in Figure 4.

as demonstrated by the (BAESBT)PbI_4 hybrid perovskite obtained with the related bifunctional molecule. It is known that the perovskite sheet, which is in part stabilized by the hydrogen bonding at the interface in hybrids, is not so robust, and that, in addition to the shape of the organic molecule, several competitive forces must be considered for the formation of perovskites. In $(AESBT)_4Pb_3I_{10}$, the organic molecules adopt a head to tail arrangement, which, we can speculate, may exist in solution just before the crystallization processon account of $\pi-\pi$ interactions and the existence of a dipolar moment due to the asymmetry of the molecule (Figures 3 and 4b). It must be noted that this result differs from the perovskite structural model proposed for materials based on monoammonium "complex" molecules (azobenzene,[15] pyrene,[16] and naphthalene[17] derivatives), from the 00*l* reflections of powder X-ray patterns.

$(AESBT)_4Pb_3I_{10}$ crystallizes in the *Pna*2_1 acentric space group and the asymmetric unit consists of four molecules and a Pb_3I_{10} trimeric unit. As a consequence of the head to

(14) Mitzi, D. B. *Chem. Mater.* **1996**, *8*, 791.

(15) Era, M.; Miyake, K.; Yoshida, Y.; Yase, K. *Thin Solid Films* **2001**, *393*, 24.

(16) Braun, M.; Tuffentsammer, W.; Wachtel, H.; Wolf, H. C. *Chem. Phys. Lett.* **1999**, *307*, 373.

(17) Era M.; Maeda, K.; Tsutsui, T. *Thin Solid Films* **1998**, *331*, 285.

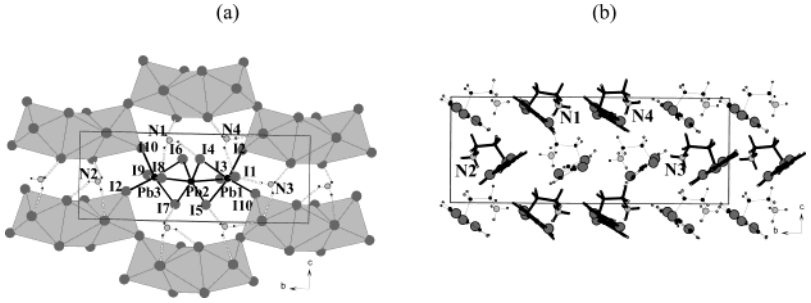

Figure 4. Views along the [−1 0 0] direction of (a) one inorganic sheet (indicated by bracket marked "*" in Figure 3) and (b) one organic sheet (indicated by bracket "**" in Figure 3) encountered in $(AESBT)_4Pb_3I_{10}$. The ammonium parts of organic molecules at the organic−inorganic interface of these two last sheets also appear in (a) together with hydrogen bonding ((*d*(H...I) in the range 2.78−3.05 Å). In (b), the bonds of molecules which interact via H bonds to the inorganic sheet shown in (a) are drawn in bold.

tail situation of molecules, a decrease of the cationic charge density at the interface occurs, involving a condensation of lead octahedra and in this case the formation of a new $Pb_3I_{10}^{4-}$ bidimensional iodoplumbate framework. An extensive work of Krautscheild et al. has been recently devoted to the synthesis of non primary ammonium salts with iodoplumbate or iodostannate anions. Thus, discrete anions and one- and two-dimensional polymeric anions have been evidenced for example in $[Bu_3N(CH_2)_4NBu_3]_4[Pb_7I_{22}]$, $[PrN(C_2H_4)_3NPr]_4[Pb_2I_6]$, and $[Me_3N\text{-}C_2H_4\text{-}NMe_3]_2[Pb_2I_7]$, respectively.[18−20] The $Pb_3I_{10}^{4-}$ anion itself has been characterized as a discrete anion in $[Bu_3N(CH_2)_4NBu_3]_2[Pb_3I_{10}]$,[18] or as a one-dimensional polymeric anion in $[Me_3N(CH_2)_5NMe_3]_2[Pb_3I_{10}]$[21] and $[NH_3(CH_2)_4CH(CH_3)NH_3][Pb_3I_{10}]$,[22] while a $Sn_3I_{10}^{3-}$ two-dimensional polymeric anion is encountered in $[Me_3PhN]_4[Sn_3I_{10}]$.[21] All these results show the wide diversity of inorganic frameworks obtained by the condensation of lead(II) (or tin(II)) octahedra, and in a way confirm that the polymeric perovskite anion in hybrids is achieved only when the ammonium cation possesses some defined characteristics, as mentioned before. The $Pb_3I_{10}^{3-}$ polymeric anion in $(AESBT)_4Pb_3I_{10}$ can be described from non centrosymmetrical units of three face-sharing octahedra linked together by iodized vertexes, two iodine atoms of the trimeric unit being linked to a lead atom only (Figure 4a). This new framework can be compared to the one evidenced in $[Me_3PhN]_4[Sn_3I_{10}]$ for the $Sn_3I_{10}^{4-}$ anion, this last being nevertheless constructed from centrosymmetrical trimeric units.[21] The Pb(1) and Pb(3) octahedra show two kinds of bond distances, three Pb−I_o distances (mean value of 3.278 Å) and three Pb−I_i shorter distances (mean value of 3.128 Å), I_o and I_i being, respectively, the outer and the inner iodide atoms of the trimeric unit (Figure 4a, Table 3). The central octahedron displays four bond distances of approximately 3.166 Å and two longer ones of 3.278 Å (Table 3). The I−Pb−I bond angles of lead octahedra are in the range of 81−103° (adjacent iodide) and 162−177° (opposite iodide), as reported in Table 3. All these values are close to those encountered in the previously quoted iodoplumbate salts. Finally, the resulting trimeric units are linked together to form a corrugated layer with a dihedral angle between the mean planes of two consecutive trimers along *b* of 58°.

The bithiophene parts of the four independent organic cations are nearly planar, all adopting an anti conformation. The organic layer also appears corrugated with the ammonium parts of molecules pointed in the holes defined by the inorganic framework (Figures 3 and 4). As in perovskite hybrids, each ammonium group interacts via hydrogen bonds to three iodine atoms, with *d*(H...I) in the range 2.70−3.05 Å (Figure 4a).

$(AESBT)_3Bi_2I_9$. The introduction of a metal at the +III oxidation state (bismuth^{III}) in the iodometalate inorganic part has also been considered in the case of the monoammonium cation. The bismuth iodide based hybrids are interesting because of the potentially semiconducting character of the inorganic framework,[23,24] as well as the rich structural diversity of these frameworks.[25] Recently, the first metal-deficient perovskite sheet ($Bi_{0.66}I_4^{2-}$) has been stabilized in a hybrid containing organic layers of quaterthiophene derived dications.[26]

$(AESBT)_3Bi_2I_9$ crystallizes in the $P2_12_12_1$ acentric space group and the asymmetric unit contains a pair of iodized-face-sharing bismuth octahedra and three organic cations in which the bithiophene parts are nearly planar, all adopting an anti conformation. The layered structure is built up from regular organic layers in which a head to tail situation of molecules occurs, separated by the inorganic sheets of $Bi_2I_9^{3-}$ dimeric units of face-sharing octahedra (Figure 5). The dihedral angle between the (a,b) plane and the bithiophene plane is 49°.

The $Bi_2I_9^{3-}$ anion has already been described previously in secondary ammonium salts,[27−29] and here displays, as expected, $Bi-I_{terminal}$ bond lengths (mean value of 2.938 Å), significantly shorter than the $Bi-I_{bridging}$ bond lengths (mean

(18) Krautscheild, H.; Vielsack, F. *J. Chem. Soc., Dalton Trans.* **1999**, *16*, 2731.
(19) Krautscheild, H.; Lode, C.; Vielsack, F.; Vollmer, H. *J. Chem. Soc., Dalton Trans.* **2001**, *7*, 1099.
(20) Krautscheild, H.; Vielsack, F.; Klaassen, N. *Z. Anorg. Allg. Chem.* **1998**, *624*, 807.
(21) Lode, C.; Krautscheild, H. *Z. Anorg. Allg. Chem.* **2001**, *627*, 1454.
(22) Bonamartini, A.; Ferrari, A. M.; Pellacani, G. C.; Saccani, A.; Sandrolini, F.; Sgarabotto, P. *Inorg. Chem.* **1999**, *38*, 716.
(23) Belotskii, D. P.; Timofeev, V. B.; Antipov, I. N.; Vashchenko, V. I.; Bespal'chenko, V. A. *Russ. J. Phys. Chem.* **1968**, *42*, 740.
(24) Fisher, G. *Helv. Phys. Acta* **1961**, *34*, 827.
(25) Fisher, G. A.; Norman, N. C. *Adv. Inorg. Chem.* **1994**, *41*, 233.
(26) Mitzi, D. B. *Inorg. Chem.* **2000**, *39*, 6107.
(27) Gridunova, G. V.; Ziger, E. A.; Koshkin, V. M.; Struchkov, Y. T.; Shklover, V. E. *Russ. J. Inorg. Chem.* **1988**, *33*, 977.
(28) Lazarini, F. *Acta Crystallogr., Sect. C* **1987**, *C43*, 875.
(29) Kawai, T.; Shimanuki, S. *Phys. Stat. Solidi B* **1993**, *177*, K43.

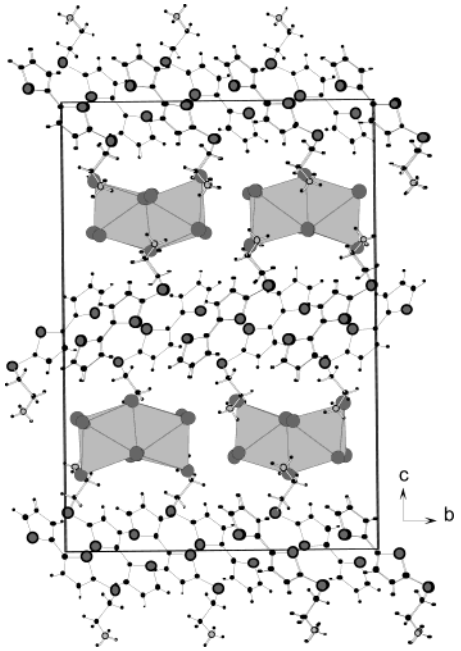

Figure 5. Layered crystal structure of $(AESBT)_3Bi_2I_9$.

value of 3.256 Å). However, in the studied compound, some uncommon degree of asymmetry exists for the bridging iodide, with bond lengths ranging from 3.200(1) to 3.366(1) Å for Bi(2) (Table 4). The deviations from regular octahedra also concern the I−Bi−I bond angles with $I_{terminal}$−Bi−$I_{terminal}$ angles greater than 90° (mean value of 94.55°) and $I_{bridging}$−Bi−$I_{bridging}$ angles shorter than 90° (mean value of 84.01°) (Table 4). This latter distortion in angle could be interpreted as the beginning of localization of the lone pairs trans to the Bi−Bi vector, and/or a geometric arrangement to minimize the Bi−Bi interaction.[25] While the reported known salts are constructed from the alternation of $Bi_2I_9^{3-}$ anions and cations in a chessboard fashion, with the shortest I...I inter-ion contacts of 4.410(2) Å in $(C_5H_{10}NH_2)_3Bi_2I_9$[27] and 4.30(1) Å in $(NH_2(C_2H_5)_2)_3Bi_2I_9$[28] for instance, inorganic sheets of $Bi_2I_9^{3-}$ anions are sandwiched between the organic layers in $(AESBT)_3Bi_2I_9$. In this sheet, closer I....I interactions of 4.065(1) Å and 4.051(1) Å for I(3)...I(1) and I(9)...I(7), respectively, are evidenced. These quite short values, slightly shorter than twice the iodine atom van der Waals radius (2.15 Å), can be explained by the hydrogen bonding at the organic−inorganic interface of this layered structure. As shown in Figure 6, the ammonium parts of molecules point in the holes of the inorganic sheet and are each linked at iodine atoms (d(H...I) in the range 2.88−3.07 Å) of both $Bi_2I_9^{3-}$ anions, leading to bring the anions together.

Molecular Packing. The field of organic semiconductors is currently investigated because of the charge transport properties and the potential application in optoelectronic devices. The thiophene oligomer family (nTs) is one of the most extensively studied since the discovery of the high field effect mobility measured in thin film transistor based on α-sexithiophene (α-6T).[9a,30] More recently, a large effort has been devoted to the synthesis of crystals and the determination of their structures.[31,32] For instance, it has been evidenced that all unsubstituted nTs (from 2T to 8T) pack according to the herringbone molecular arrangement, also called α-type plane, and that promising charge-transport properties are expected in material based on oligomer containing at least four thiophene units. In this current work, the bithiophene derived molecules incorporated in hybrids constitutes a model molecule to demonstrate that organic−inorganic hybrid structures provide a good opportunity to achieve new well-ordered oligothiophene organic layers.

In the triclinic structure of $(BAESBT)PbI_4$, the long axes of the molecules are not exactly parallel to each other, leading to an irregular molecular packing (Figure 7). Also, taking into account the statistical disorder, two molecular packings can be considered, the one with the major component of the disordered molecule (Figure 7a), the other with the minor component (Figure 7b). In this last packing, all molecules

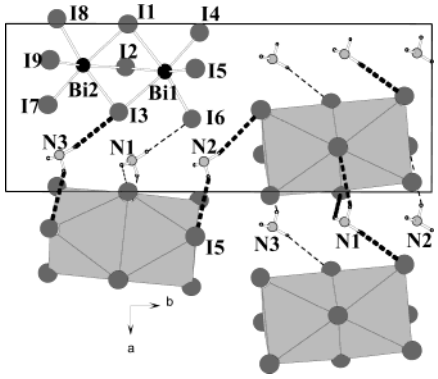

Figure 6. View along a of the $Bi_2I_9^{3-}$ anions building the inorganic sheet in $(AESBT)_3Bi_2I_9$. The numbering scheme also appears on this figure along with the ammonium parts of molecules involved in hydrogen bonding (d(H...I) in the range 2.88−3.07 Å) at the organic−inorganic interface between the inorganic sheet and the two neighboring organic layers. Hydrogen bonds that take place at the same side of the inorganic sheet are drawn alike.

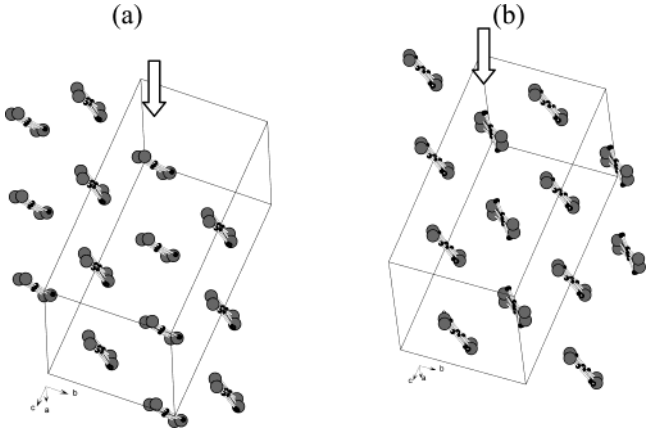

Figure 7. View down the long molecular axis of one layer of cations in $(BAESBT)PbI_4$ when the major component (a) or the minor component (b) of the disordered molecule is considered. The arrows indicate the columns built up from the disordered molecules. For clarity, the ethylammonium parts of cations have not been drawn.

(30) Horowitz, G.; Garnier, F.; Yassar, A.; Hajlaoui, R.; Kouki, F. *Adv. Mater.* **1996**, *8*, 52.

(31) Fichou, D. *J. Mater. Chem.* **2000**, *10*, 571.

(32) Antoini, L.; Horowitz, G.; Kouki, F.; Garnier, F. *Adv. Mater.* **1998**, *10*, 382.

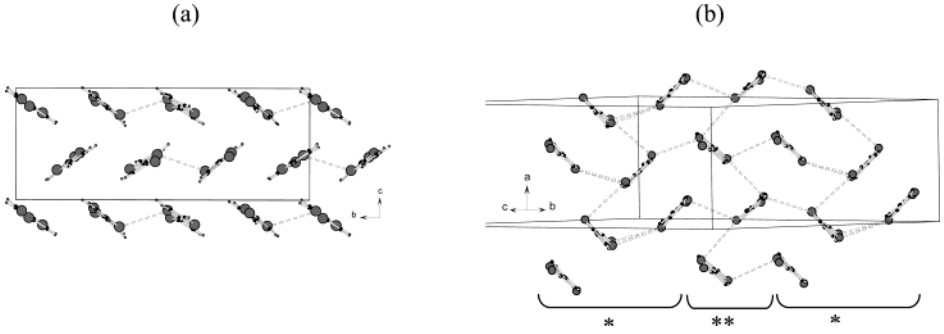

Figure 8. View down the long molecular axis of one layer of cations in $(AESBT)_4Pb_3I_{10}$ (a) and in $(AESBT)_3Bi_2I_9$ (b). A herringbone molecular arrangement is found in $(AESBT)_4Pb_3I_{10}$ (a), whereas the bithiophene units form a mixed molecular packing where a so-called κ molecular arrangement (shown by the bracket "*" in (b)) alternates with a herringbone molecular arrangement (shown by bracket "**"). Dashed lines are drawn for S...S distances smaller than 3.90 Å, and the ethylammonium parts of cations have been omitted for clarity.

Table 5. Shortest Intermolecular Contacts in $(BAESBT)PbI_4$, $(AESBT)_4Pb_3I_{10}$, and $(AESBT)_3Bi_2I_9$, Together with Those Reported in $(AEQT)PbBr_4$ and α-6T for Comparison[a]

	$(BAESBT)PbI_4$	*$(AEQT)PbBr_4$* [ref 8]	$(AESBT)_4Pb_3I_{10}$	$(AESBT)_3Bi_2I_9$	*α−6T* ref 34]
d(S....S) in Å	3.92(1) S(1)....S(4)	*4.148(3)*	3.86(1) S(6)....S(8)	3.729(6) S(2).....S(5)	*4.18*
d(S...C) in Å	3.68(3) S(1)....C(10)	*3.580(9)*	3.52(4) S(7)*....C(29)	3.807(2) S(8)....C(15)	*3.91*
d(C...C) in Å	3.49(4) C(3)....C(11)	*3.586(8)*	3.58(4) C(23)....C(28)	3.55(1) C(15)....C(19)	*3.67*

[a] All enumerated atoms belong to the bithiophene unit except the one with an asterisk (*).

appear approximately parallel, forming a so-called β-type sheet. The description of the second packing is deduced from the first one by considering, from a geometric point of view, a slight rotation of the disordered molecules along their long molecular axis (Figure 7a). These arrangements of the bithiophene units are probably the result of both effects of the sulfur ethylammonium tethering group and the hydrogen bonding at the organic−inorganic interface, and appear different from the herringbone type sheets evidenced in purely organic compounds of the nTs family or in the $(AEQT)PbBr_4$ hybrid containing quaterthiophene units (AEQT = $NH_3C_2H_5$-QT-$C_2H_5NH_3$). It must be noted that the β-type molecular packing is often encountered in cation radical salts of the BEDT-TTF series (BEDT-TTF = bis(ethylendithio) tetrathiafulvalene).[33]

A view along the long molecular axis of an organic layer of the $(AESBT)_4Pb_3I_{10}$ and $(AESBT)_3Bi_2I_9$ structures is given in Figure 8. In $(AESBT)_4Pb_3I_{10}$, a herringbone molecular packing occurs. The shortest S...S intermolecular contacts are found to be in the pairs of molecules for which the corresponding ammonium parts point in the same hole defined by the $Pb_3I_{10}^{4-}$ framework (Figure 4), underlining the influence of the inorganic sheet. The interplay between the organic and inorganic parts is even better demonstrated in the structure of $(AESBT)_3Bi_2I_9$. While molecules bearing the $N(2)H_3^+$ ammonium groups, which interact with two $Bi_2I_9^{3-}$ anions along b (Figure 6), form columns (along a) with a herringbone molecular arrangement, molecules bearing $N(1)H_3^+$ and $N(3)H_3^+$ ammonium groups are faced with a head to tail situation, defining, along a, columns of dimers perpendicular from each other (Figure 8b). This last arrangement, the so-called κ molecular arrangement, is especially well-known in the field of organic conductors because the highest Tc superconductors in the BEDT-TTF series are built up from such sheets. In Table 5, the shortest intermolecular contacts observed in the hybrids described in this paper are reported, together with those given in the literature for $(AEQT)PbBr_4$ [8] and α-6T.[34] These values can give good indications of charge-transport properties in the corresponding organic layers, even if the orbital overlap mode must also be considered. For the drawing of S...S contacts (Figure 8), the limit value has been chosen as 3.9 Å. This value is higher than twice the van der Waals radius of the sulfur atom, but shorter contacts are uncommon in neutral-molecules-based organic compounds. Compared to $(AEQT)PbBr_4$ or α-6T compounds, some shorter intermolecular contacts are found in the new hybrids, especially in $(AESBT)_3Bi_2I_9$ where a bidimensional network of S...S intermolecular contacts is evidenced (Figure 8b, Table 5).

Physical Properties. The optical spectra were recorded at room temperature on crystallized films of $(BAESBT)PbI_4$, $(AESBT)_4Pb_3I_{10}$, and $(AESBT)_3Bi_2I_9$ (Figure 9). In $(BAESBT)PbI_4$, the observed exciton peak at 504 nm is characteristic of the inorganic sheets of corner-sharing lead(II) iodide octahedra, whereas in $(AESBT)_4Pb_3I_{10}$ the peak associated to the $Pb_3I_{10}^{4-}$ corrugated inorganic framework is blue shifted to 422 nm. For the bismuth compound, a clear exciton peak is observed at 498 nm, a value close to that of $(CH_3NH_3)_3Bi_2I_9$ (λ = 494 nm).[29]

The room-temperature photoluminescence emission spectrum (λ_{exc} = 457 nm) of $(BAESBT)PbI_4$ reveals no peak, contrary to what is observed in hybrid perovskites based on PbI_4^{2-} sheets and optically inert organic molecules (alkyl or simple aromatic molecules). As already shown for $(AEQT)PbI_4$,[8] charge transfer between the two components, due to

(33) Williams, J. M.; Ferraro, J. R.; Thorn, R. J.; Carlson, K. D.; Geiser, U.; Wang, H. H.; Kini, A. M.; Whangbo, M. H. *Organic Superconductors*; Prentice Hall: Englewood Cliffs, NJ, 1992.

(34) Horowitz, G.; Bachet, B.; Yassar, A.; Lang, P.; Demanze, F.; Fave, J. L.; Garnier, F. *Chem. Mater.* **1995**, *7*, 1337.

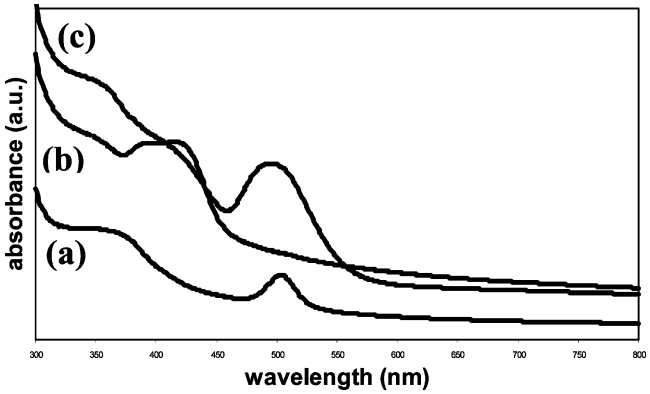

Figure 9. UV−VIS absorption spectra of crystallized films of (BAESBT)-PbI_4 (a), $(AESBT)_4Pb_3I_{10}$ (b), and $(AESBT)_3Bi_2I_9$ (c) at room temperature.

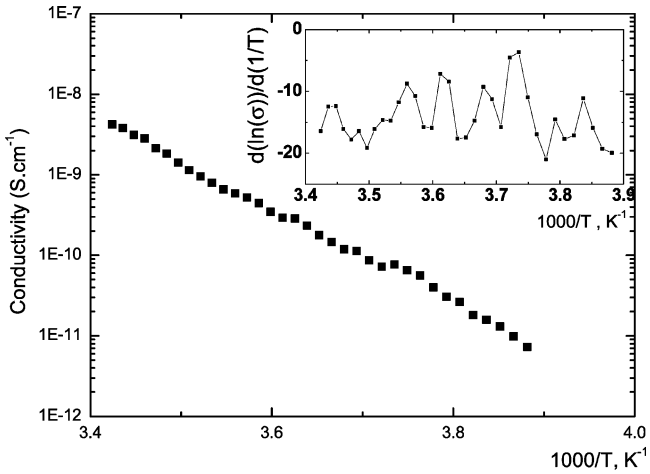

Figure 10. Evolution of conductivity of a (BAESBT)PbI_4 single crystal as a function of reciprocal absolute temperature. Inset: plot of $d(\ln(\sigma))/d(1/T)$ to check the activated behavior of the conductivity. Deviations from the horizontal line are due to electrical noise amplified by the calculation of the derivative.

a relative shift of the PbI_4^{2-} band gap and the bithiophene HOMO−LUMO gap, could explain the luminescence quenching of the inorganic part. Similarly, both $(AESBT)_3Bi_2I_9$ and $(AESBT)_4Pb_3I_{10}$ ($\lambda_{exc} = 355$ nm) do not exhibit any photoluminescence.

Large crystals of (BAESBT)PbI_4 were obtained, allowing measurement of the electrical conductivity. Figure 10 shows the electrical conductivity, σ, of one (BAESBT)PbI_4 single-crystal submitted to an electric field $F = 16$ kV/cm. As shown in the inset, $d(\ln(\sigma))/d(1/T)$ is roughly temperature independent; conduction in (BAESBT)PbI_4 is then dominated by thermally activated processes. The apparent activation energy corresponds to a characteristic energy $E_g = 2.535$ eV so a characteristic wavelength $\lambda = 490$ nm. This value is similar to the exciton energy deduced from UV−Vis absorption spectra performed on this compound (Figure 9). This similarity is in favor of a conduction confined along the inorganic PbI_4^{2-} layers. Finally, the transport within the planes is investigated in Figure 11 for a (BAESBT)PbI_4 single crystal in the dark at ambient temperature. At low electric field, an Ohmic behavior is obtained. A further increase of the applied current leads to a crossover to a quadratic dependence of the current on the applied electric

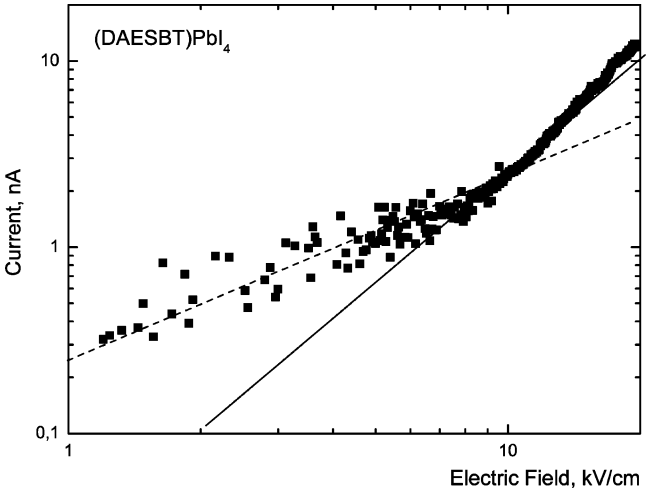

Figure 11. Evolution of the dark current of a (BAESBT)PbI_4 single crystal as a function of the applied electric field, applied along the layers, at room temperature. The dashed line is a fit to an Ohmic behavior (current proportional to the electric field) whereas the solid line represents a fit to a F^2 dependence.

Scheme 1. Schematic Route to (AESBT)Cl and $(BAESBT)Cl_2$[a]

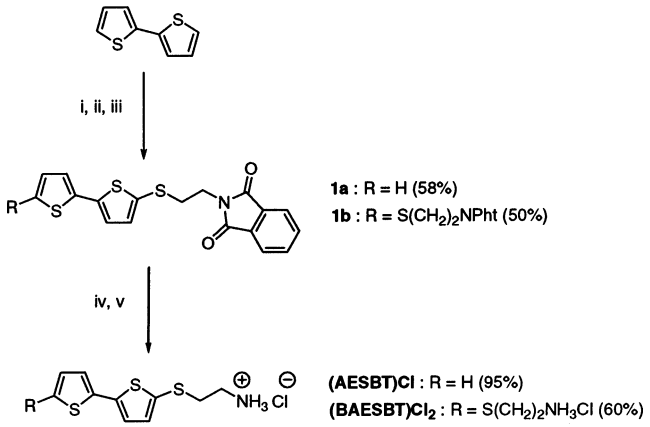

[a] (i) *n*-BuLi (1.05 equiv), THF, −78 °C, 30 min for **1a** or *n*-BuLi (2.1 equiv), THF, −78 °C (30 min) to room temperature (1 h) for **1b**. (ii) S_8 (1.05 equiv), −78 °C (30 min) to 0 °C for **1a** and S_8 (2.1 equiv), rt (1 h) for **1b**. (iii) *N*-(2-bromoethyl)phthalimide, 0 °C. (iv) $NH_2NH_2 \cdot H_2O$, THF-EtOH, reflux. (v) 6 N HCl in $CHCl_3$ or THF, respectively, for (AESBT)Cl or $(BAESBT)Cl_2$.

field. This behavior of the current versus the applied electric field is commonly observed in semiconductors using a standard semiconductor model and is usually interpreted in terms of a space-charge limited conduction at intermediate electric fields.[35] We notice that the measured dark current is larger than the dark current reported in the similar compound PhE-Pb_2I_7.[36] Further investigations of conduction in these materials are needed.

Conclusion

Hybrid materials based on iodometalate 2,2′ bithiophene derivatives bearing one or two ammonium groups have been synthesized. In the Pb/I system, the hybrid perovskite (BAESBT)PbI_4 has been identified when formed from the diammonium cation, whereas a head to tail arrangement of

(35) Smith, R. W.; Rose, A. *Phys. Rev.* **1955**, *97*, 1531.
(36) Hong, X.; Ishihara, T.; Nurmikko, A.V. *Solid State Commun.* **1992**, *84*, 657.

the molecules occurs with the monoammonium cation, precluding the formation of the hybrid perovskite but leading to a new inorganic framework $(AESBT)_4Pb_3I_{10}$ compound. A similar situation of organic molecules has been observed in the case of the $(AESBT)_3Bi_2I_9$ layered compound. These three salts have been obtained as crystals, and can also be processed into thin films by spin-coating.

Whereas unsubsituted nTs oligomers always pack in a herringbone fashion in the related solids, many molecular packing types as hybrid structures have been evidenced here, underlining the influence of the nature of the cation, of the inorganic part, and of their interface on the material organization. This interplay between organic and inorganic components is thus well demonstrated for $(AESBT)_3Bi_2I_9$ where an original mixed kappa-alpha type arrangement of the bithiophene units is correlated to the inorganic $Bi_2I_9^{3-}$ anionic framework. Furthermore, molecular interactions, especially of S....S type, seem to be stronger in the hybrids based on the monoammonium cations.

Such monocations appear well suited to synthesize new, eventually more dense, ordered organic layers in these halogenometalate hybrids.

Acknowledgment. We thank Pays de la Loire region for a post-doc fellowship to X.H.Z.

Supporting Information Available: Listings of crystallographic data, atomic coordinates, and anisotropic motion parameters; powder XRD patterns of bulk samples of $(BAESBT)PbI_4$, $(AESBT)_4Pb_3I_{10}$ and $(AESBT)_3Bi_2I_9$; and ^1H NMR spectra of compounds 1a, 1b, (AESBT)Cl, and $(BAESBT)Cl_2$ (PDF). Crystallographic information files (CIF). This material is available free of charge via the Internet at http://pubs.acs.org.

IC034235Y